The Astrophysical Journal, 652:793–799, 2006 November 20
© 2006. The American Astronomical Society. All rights reserved. Printed in U.S.A.

# A TRIGGER MECHANISM OF MAGNETIC RECONNECTION AND PARTICLE ACCELERATION DURING THINNING OF THE CURRENT SHEET

S. Saito and J. I. Sakai
Laboratory for Plasma Astrophysics, Faculty of Engineering, University of Toyama, 3190, Gofuku, Toyama 930-8555, Japan
*Received 2006 March 20; accepted 2006 August 8*

## ABSTRACT

One of the trigger mechanisms of magnetic reconnection in the compressing current sheet is studied by using a two-dimensional full particle-in-cell code modified from the TRISTAN code. In the compressed current sheet, the electrons are heated preferentially perpendicular to the magnetic field due to adiabatic heating. The thinning and anisotropy $T_\perp/T_\parallel$ of electrons in the current sheet vigorously enhance the tearing instability with several small-scale magnetic islands. The generated magnetic islands successively coalesce and the magnetic energy is converted into plasma kinetic energy. Through the coalescence, high-energy electrons are quasi-periodically produced. At almost the same time, some ions are accelerated by the magnetosonic shock waves generated around the current sheet. The acceleration sites for the ions move the outside of the current sheet. At the final stage, all magnetic islands merge into a large one whose width is about 10 times larger than the compressed sheet width. The thinning of the current sheet leads to the generation of large-scale magnetic islands and converts the magnetic field energy into kinetic energy of the plasma. The dynamical evolution of current sheets can be applied to solar flares.

*Subject headings:* Sun: flares — Sun: magnetic fields

## 1. INTRODUCTION

Solar flares explosively release the energy stored in the corona, involving plasma heating, particle acceleration, and electromagnetic radiation. It is widely accepted that the main energy source is the magnetic field. The magnetic energy is rapidly converted through the magnetic reconnection process. A part of the released energy accelerates both electrons and ions to high energies during a flare event. Recent observation (Hurford et al. 2003) with the *Reuven Ramaty High-Energy Solar Spectroscopic Imager* (*RHESSI*) implied a difference in acceleration and/or propagation between the accelerated electrons and ions. It is important to find causes for the difference between them in order to understand acceleration mechanisms in solar flares.

Magnetic reconnection occurs in the current sheet through resistive effects or the microinstabilities after the current sheet is formed at several locations that depend on the plasma flow and magnetic field configuration. Especially in the collisionless plasma, the current sheet leads to instabilities, such as the collisionless tearing instability, the lower hybrid drift instability, and the Weibel instability. These instabilities could be parts of an important onset mechanism for the fast magnetic reconnection. One of the instabilities in the current sheet, the tearing instability, has been a candidate for the onset of magnetic reconnection. However, the influence of the tearing instability in collisionless plasma is too weak to cause the magnetic reconnection that leads to a sudden energy release. Other processes may be needed to vigorously enhance the tearing instability. The onset mechanism of the magnetic reconnection is one of the problems concerning solar flares.

One of the candidates for onset mechanisms is temperature anisotropy in the current sheet. The anisotropic tearing instability has been investigated by some authors (Ambrosiano et al. 1986; Hewett et al. 1988; Burkhart & Chen 1989; Karimabadi et al. 2004). The anisotropy $T_\perp/T_\parallel > 1$ in the current sheet strongly enhances the tearing instability with several magnetic islands smaller than isotropic tearing, where the subscripts $\perp$ and $\parallel$ indicate the directions perpendicular and parallel to the magnetic field. Therefore, it is important to study how the temperature anisotropy grows in the current sheet. Recent studies (Daughton et al. 2004) indicated that nonlinear development of the lower hybrid drift instability (LHDI) can heat the electrons preferentially perpendicular to the magnetic field in the equilibrium current sheet. Ricci et al. (2004) have studied it in a three-dimensional system. They found that the LHDI strongly modified the linear and nonlinear evolution of the tearing instability. They studied the onset mechanism of magnetic reconnection in the equilibrium current sheet. Now we pay attention to studying the onset mechanism of the magnetic reconnection. We consider the dynamical current sheet before the solar flare. If the nonequilibrium current sheet has the temperature anisotropy $T_\perp/T_\parallel > 1$, it could strongly lead to the tearing instability and the onset of magnetic reconnection in the unstable, dynamical current sheet.

In this paper, we study the onset mechanism of magnetic reconnection in the current sheet with uniform compression by using the two-dimensional PIC code. In this simulation we find the electron temperature anisotropy $T_\perp/T_\parallel = 2.1$ in the uniformly compressed current sheet. The anisotropy works as the driver of the tearing instability. The generated small-scale magnetic islands interact with each other and heat the electrons in the current sheet. The generated islands merge into a large island whose width is about 10 times larger than the compressed sheet. The generated large islands may lead to large-scale magnetic reconnection and release the magnetic energy. We emphasize that we have to consider not only the instabilities in the stable current sheet but also the compressing stage of the unstable current sheet for an onset of the magnetic reconnection. In § 2 we show the simulation model and the initial condition. The simulation results are shown in § 3. We conclude in § 4.

## 2. SIMULATION MODEL AND INITIAL CONDITIONS

A two-dimensional, fully electromagnetic relativistic particle-in-cell code modified from the TRISTAN code (Buneman 1993) is used for this study. The number of grids for the simulation box is $L_x \times L_y = 1050 \times 2000$. The boundary condition for the

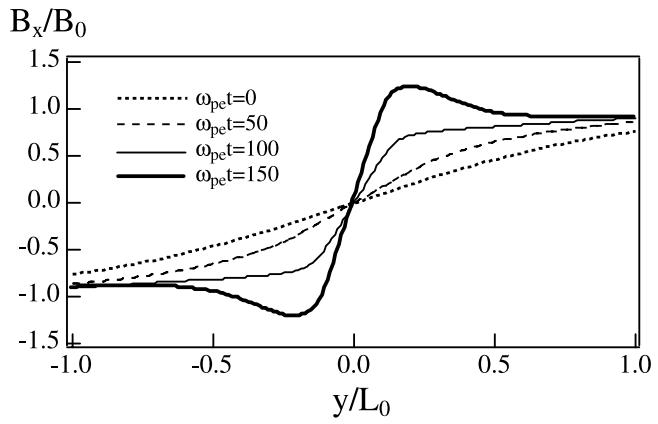



FIG. 1.—Magnetic field $B_x/B_0$ along the $y$-axis with $x = 5L_0$ at $\omega_{pe}t = 0$ (*dotted line*), 50 (*dashed line*), 100 (*solid line*), and 150 (*bold solid line*). The horizontal axis normalized by the initial sheet width $L_0$ indicates the $y$-direction, where the magnetic neutral point is located at $y = 0.0$.

particles and field is periodic in the $x$-direction. The free boundary condition is imposed for the field at the $y$-boundary, and particles at the $y$-boundary are taken away from the simulation box. Conversely, an appropriate number of particles are injected from the $y$-boundary to the simulation box. The initial magnetic field and plasma current for the initial current sheet are $B_x = B_0 \tanh(y/L_0)$ and $J_z = J_0 \cosh^{-2}(y/L_0)$, where $L_0$ is the initial sheet width. The initial velocity distributions are shifted Maxwellians with the thermal velocity $v_{\mathrm{th},s} = (T_s/m_s)^{1/2}$, the drift velocity for plasma current $U_{z,s} = J_z/(2n_0q_s)$, and the drift velocity for plasma inflow $U_y = -0.5v_{\mathrm{A}} \tanh(y/L_0)$, where $T_s$ is temperature, $m_s$ is the mass, $q_s$ is the charge, $n_0$ is the number of ion-electron pairs per cell, $v_{\mathrm{A}}$ is Alfvén velocity, and $s = i, e$ for ion, electron. The electric field $E_z = -U_yB_x$ is put in the system for the initial condition. The electric field appears when the plasma moves perpendicular to the magnetic field. The plasma inflow uniformly compresses the current sheet from both the upper and lower sides. The parameters for this simulation are $\omega_{pe}\delta t = 0.05$, $\lambda_{\mathrm{D},e}/\Delta = 1$, and $m_i/m_e = 64$, where $\omega_{pe}$, $\delta t$, $\lambda_{\mathrm{D},e}$, and $\Delta$ are electron plasma frequency, time step, electron Debye length, and grid size, respectively. The electron skin depth is $c/\omega_{pe} = 10\Delta$. There is an artificial parameter $m_i/m_e = 64$ because of the limitation of computational power. Future plans call for a simulation with a real mass ratio $m_i/m_e = 1836$. The other parameters associated with the magnetic field $B_0$ are $\rho_i/(c/\omega_{pe}) = 1.265$, $\rho_e/(c/\omega_{pe}) = 0.158$, $v_{\mathrm{A}}/v_{\mathrm{th},i} = 6.32$, $\omega_{ce}/\omega_{pe} = 0.632$, and plasma $\beta = 0.05$, where $\rho$ is the Larmor radius. In this simulation, the initial width for current sheet is $L_0 = 10(c/\omega_{pe})$ and the Alfvén transit time normalized by $\omega_{pe}$ is $\omega_{pe}t_{\mathrm{A}} = 125$, where $t_{\mathrm{A}} = L_0/v_{\mathrm{A}}$. The initial number of electron-ion pairs is $1.323 \times 10^8$. The number of pairs increases with time due to the injection of the plasma inflow with the velocity $U_y$ from the $y$-boundary. The initial temperature $T_i = T_e$ and the particle density are uniform throughout the whole system. While the initial current sheet is not stable, we accept this model because the compressing current

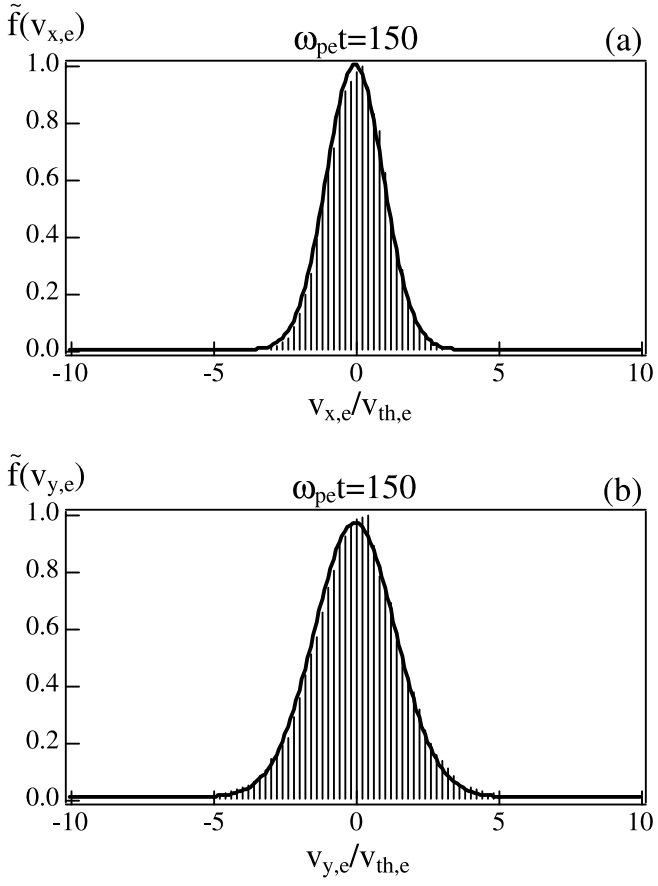



FIG. 2.—Electron velocity distribution of (*a*) $v_{x,e}/v_{\mathrm{th},e}$ and (*b*) $v_{y,e}/v_{\mathrm{th},e}$ at $\omega_{pe}t = 150$. The velocity distribution functions are normalized by each maximum value. The bold solid curve along the distribution is the fitting one with the Gaussian function $A_0 + A \exp\{-[(v - v_0)/v_{\mathrm{th}}]^2\}$.

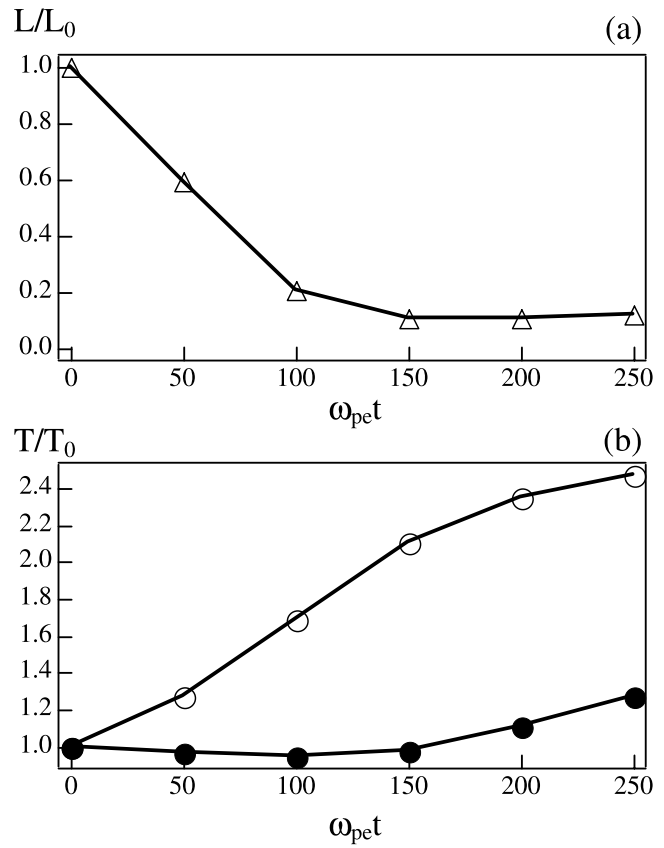



FIG. 3.—Time developments of the current sheet width and the electron temperature estimated from the electron velocity distribution around the current sheet $-0.2L_0 \le y \le 0.2L_0$ at every $\omega_{pe}t = 50$. (*a*) Time development of current sheet width is shown by triangles and a solid line. (*b*) Development of the electron temperatures $T_\perp$ and $T_\parallel$ are shown by the open circles and the filled circles, respectively, with the solid lines.

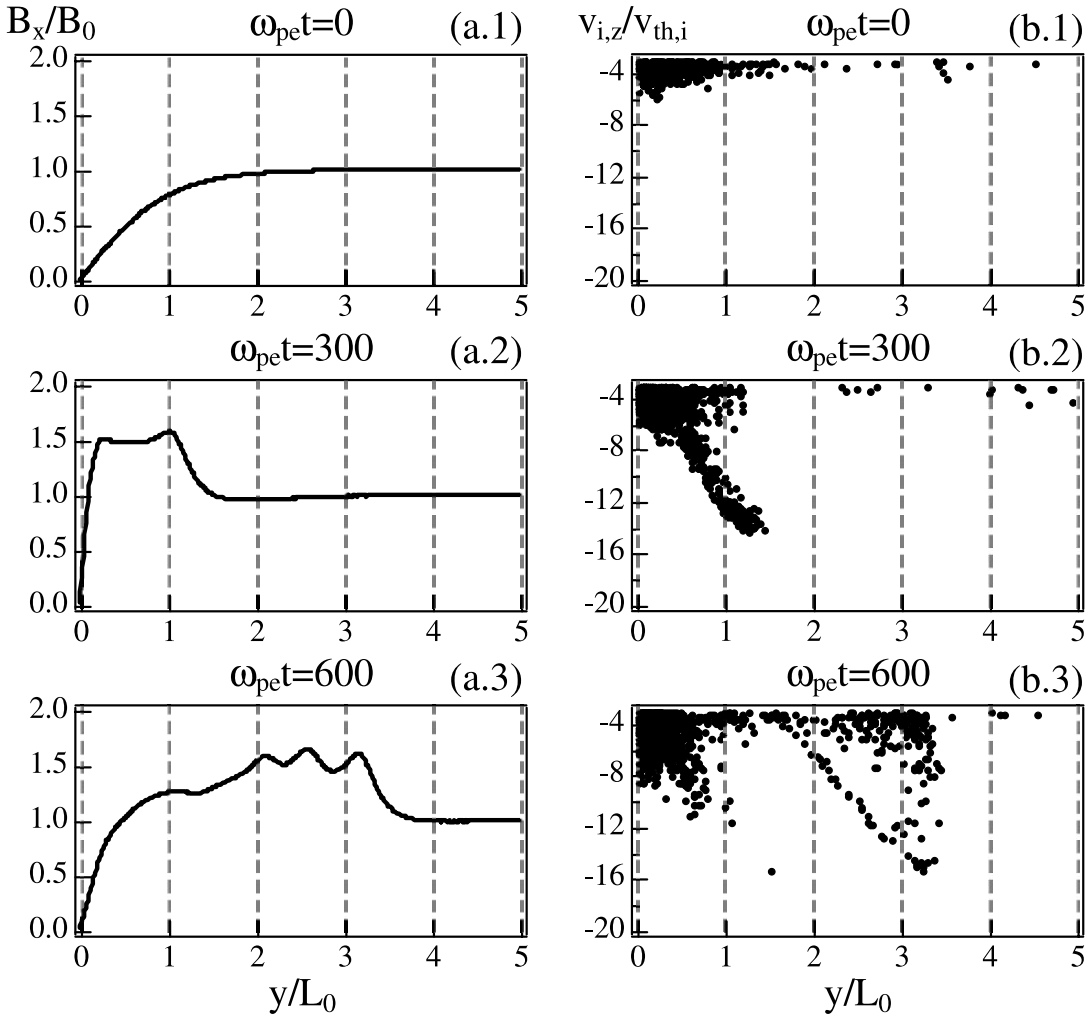



FIG. 4.—Time development of the magnetic field $B_x/B_0$ and the phase space $y/L_0$-$v_{i,z}/v_{\mathrm{th},i}$ plots for some ions at $\omega_{pe}t = 0$, 300, and 600. In (*a*.1)–(*a*.3), the magnetic field $B_x/B_0$ is plotted on the $x = 5L_0$ line between $y/L_0 = 0$ and $y/L_0 = 5$. Some ions whose velocities are larger than $3v_{\mathrm{th},i}$ are randomly picked up from the region between $y/L_0 = 0$ and $y/L_0 = 5$ in (*b*.1)–(*b*.3).

sheet could not satisfy the stable condition, especially before a flare.

## 3. SIMULATION RESULTS

In the beginning of the simulation, the current sheet is uniformly compressed by the plasma inflow from both the upper and the lower side. Figure 1 shows the magnetic field $B_x/B_0$ along the $y$-axis with $x = 5L_0$ at $\omega_{pe}t = 0$ (*dotted line*), 50 (*dashed line*), 100 (*solid line*), and 150 (*bold solid line*). As seen in the figure, the magnetic field is gradually compressed by the inflow. In other words, the current sheet gradually becomes thinner. The width of the current sheet reaches $0.1L_0$ at $\omega_{pe}t = 150$.

At the time $\omega_{pe}t = 150$, electron anisotropic heating appears in the current sheet. Figure 2 shows the electron velocity distributions of $v_{x,e}/v_{\mathrm{th},e}$ (Fig. 2*a*) and $v_{y,e}/v_{\mathrm{th},e}$ (Fig. 2*b*) at $\omega_{pe}t = 150$. The bars indicate the number of electrons at each velocity whose value is normalized by the maximum value of each velocity distribution. Ten percent of the electrons are randomly picked up from the region $-0.2 \leq y/L_0 \leq 0.2$. The bold solid line on each distribution is the fitting curve with the Gaussian function $A_0 + A\exp\{-[(v - v_0)/v_{\mathrm{th}}]^2\}$. Each fitting curve is well fitted with each velocity distribution, as seen in Figures 2*a* and 2*b*. This indicates that both velocity distributions are almost thermal distributions. The critical difference between them is the width of the distribution, which means the difference of temperature depending on the direction. From the difference of the width, the anisotropic electron temperature ratio $T_\perp/T_\parallel = 2.1$ is estimated in the current sheet.

Figure 3 shows the time development of the current sheet width $L/L_0$ and the electron temperature estimated from the electron velocity distribution in the region $-0.2 \leq y/L_0 \leq 0.2$ at every $50(\omega_{pe}t)$. The time development of the current sheet width is plotted by triangles with a solid line in Figure 3*a*, and the development of the electron temperatures $T_\perp/T_0$ and $T_\parallel/T_0$ are plotted by open circles and filled circles with solid lines in Figure 3*b*, where $T_0$ is the initial temperature. As seen in Figure 3*a*, the current sheet width linearly decreases until $\omega_{pe}t = 100$. Simultaneously, the electron temperature perpendicular to the magnetic field increases, as seen in Figure 3*b*. The temperature parallel to the magnetic field does not increase until $\omega_{pe}t = 150$. From the results in Figure 3, we expect that the correlation between the change of the magnetic field around the current sheet and the electron temperature perpendicular to the magnetic field could be associated with the adiabatic heating. The electrons around the current sheet could be heated by the electric field related to the $\partial B_x/\partial t$ component. However, we cannott apply the simple adiabatic heating process because the magnetic moment $\mu = mv_\perp^2/2B$ for the electrons is not conserved at any time in the

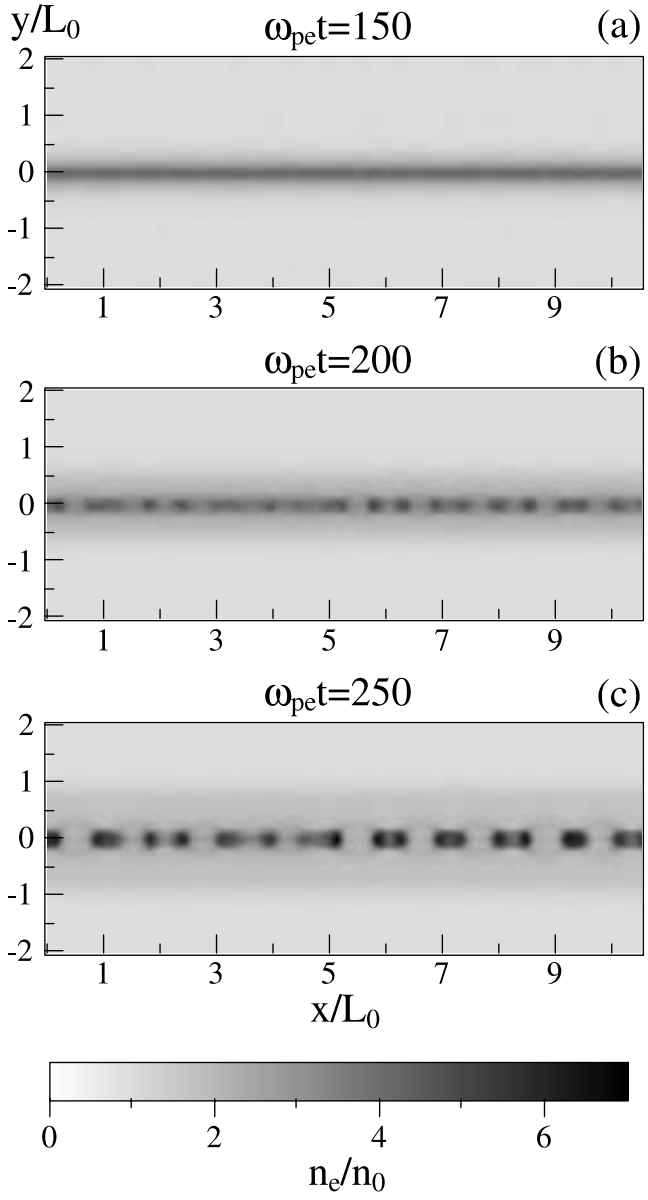



FIG. 5.—Electron density $n_e/n_0$ at $\omega_{pe}t = 150$, 200, and 250. These are plotted in the region $-2 \leq y/L_0 \leq 2$.

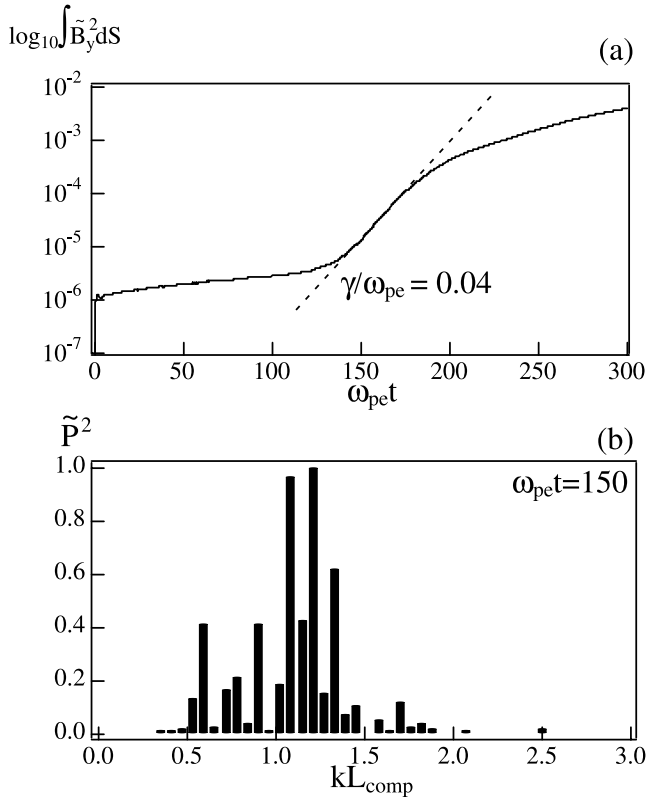



FIG. 6.—(*a*) Time development of magnetic field energy of $B_y$ component during the tearing stage. (*b*) Energy spectrum of $B_y$ component on the line $y = 0$ at $\omega_{pe}t = 150$. The horizontal axis in (*b*) shows the wavenumber normalized by the width of the compressed current sheet $L_{\rm comp}$.

current sheet. Therefore we need a more detailed study of the heating process associated with the change of the magnetic field with time in the strong magnetic gradient. In this simulation, the initial condition is not in the force balance, $\boldsymbol{J}\times\boldsymbol{B} \neq \nabla P$. We did the simulation excluding the plasma inflow. Although the current sheet was compressed by itself, the sheet width did not reach $0.1L_0$ and there was little electron temperature anisotropy in the current sheet. The result means that the energy in the current sheet is not enough to compress the current sheet and to increase the temperature anisotropy. Therefore, as compared with the simulation with the plasma inflow, the kinetic energy that comes from the outside of the current sheet could be an energy source responsible for changing the condition of the current sheet.

During the thinning of the current sheet, some ions are accelerated by the magnetosonic shocks that propagate to the outer region. Figure 4 shows the time development of the magnetic field and the phase space $y$-$v_{i,z}$ for some ions at $\omega_{pe}t = 0$, 300, and 600. In Figures 4*a*.1–4*a*.3, the magnetic field $B_x/B_0$ is plotted along the $y$-axis at $x = 5L_0$. Some ions whose velocities are larger than $3v_{{\rm th},i}$ that are randomly picked up from the region between $y/L_0 = 0$ and $y/L_0 = 5$ are shown in Figures 4*b*.1–4*b*.3. The velocity is normalized by the initial ion thermal velocity. During the thinning of the current sheet, the magnetic field is compressed and generates the magnetosonic shock wave with Alfvén Mach number $M_{\rm A} \approx 1.5$ from the current sheet, as seen in Figure 4*a*.2. The magnetosonic waves are generated on both sides of the current sheet and propagate toward the outer region. At the same time, in Figure 4*b*.2, part of ions are strongly accelerated around the region where the shock front of the magnetosonic waves are located. The acceleration site of the ions moves along with the shock front of the waves, which propagate toward the outer region, as seen in Figures 4*a*.3 and 4*b*.3. The ions trapped by the magnetosonic shock are accelerated by the surfatron mechanism. The maximum velocity of the ions accelerated by the surfatron mechanism (Ohsawa & Sakai 1987) is

$$\frac{v_{\rm max}}{v_{{\rm th},i}} = \frac{v_{\rm A}}{v_{{\rm th},i}}\left(\frac{m_i}{m_e}\right)^{1/2}(M_{\rm A}-1)^{3/2}. \qquad (1)$$

By using the equation, we obtain $v_{\rm max}/v_{{\rm th},i} = 17.8$ with the parameters $v_{\rm A}/v_{{\rm th},i} = 6.32$, $m_i/m_e = 64$, and $M_{\rm A} = 1.5$. The maximum velocity agrees well with the result from the simulation, as seen in Figures 4*b*.2 and 4*b*.3.

The time development of the compressed current sheet is shown in Figure 5. The gray scale shows the electron density normalized by $n_0$ in the region $-2 \leq y/L_0 \leq 2$ at $\omega_{pe}t = 150$, 200, and 250. At $\omega_{pe}t = 150$, the thin compressed sheet uniformly appears in the center of the system. After that, the sheet begins to be torn into small-scale magnetic islands. At $\omega_{pe}t = 250$, many

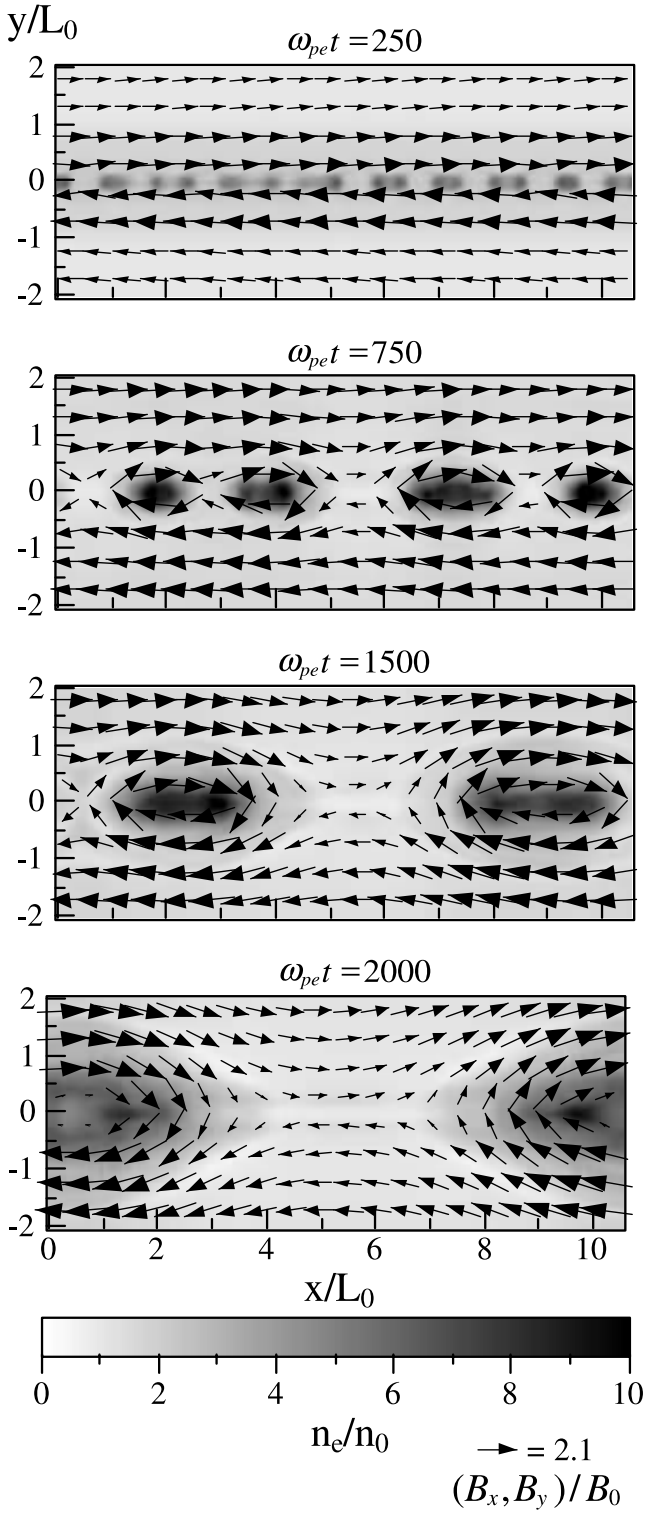



FIG. 7.—Vector plots show the magnetic field $B_x$ and $B_y$ normalized by $B_0$. The gray scale shows the electron density normalized by $n_0$ at $\omega_{pe}t = 250$, 750, 1500, and 2000. These are plotted in the region $-2 \le y/L_0 \le 2$.

small-scale islands clearly grow in the current sheet. This is the result of the collisionless tearing instability that accompanies the generation of the magnetic field $B_y$ in the current sheet. Figure 6*a* shows the time history of the magnetic field energy of $B_y$ with log scale, which is normalized by the initial magnetic field energy in the system. Figure 6*b* shows the power spectrum of $B_y$ along the center of the current sheet at $\omega_{pe}t = 150$, the value of which is

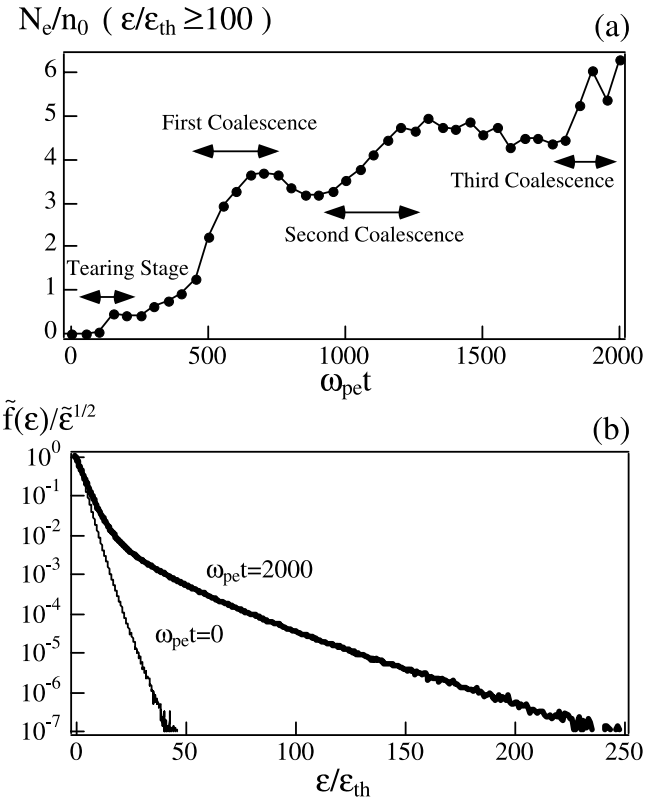



FIG. 8.—(*a*) Time history of the number of high-energy electrons in the current sheet. (*b*) Energy spectrum of the electrons at $\omega_{pe}t = 0$ and 2000. The kinetic energy is normalized by the initial electron thermal energy.

normalized by the maximum one. The horizontal axis is the wavenumber normalized by $L_{\rm comp}$, defined as $0.1L_0$, which is given in Figure 3*a* at $\omega_{pe}t = 150$. We can see the exponential growth of $B_y$, which indicates the growth of the tearing mode during the time from $\omega_{pe}t = 150$ to 170. The growth rate is $\gamma/\omega_{pe} \approx 0.04$, which is estimated from the dashed line in Figure 6*a*. As seen in Figure 6*b*, the growing modes have the wavenumber $kL_{\rm comp} \ge 1$. We expect that the enhancement of the tearing instability is related to the electron anisotropy by the sheet compression. The anisotropic tearing instability can excite the tearing modes with the wavenumbers $kL_{\rm comp} \ge 1$, which can saturate at an amplitude larger than isotropic tearing.

Figure 7 shows the nonlinear development of the current sheet. The vector plots show the magnetic field $B_x/B_0$ and $B_y/B_0$. The gray scale shows electron density $n_e/n_0$. At $\omega_{pe}t = 250$, the small-scale magnetic islands are generated in the current sheet. (The electron density profile in Fig. 5*c* is more clear.) Some islands generated by the anisotropic tearing instability merge into four islands between $\omega_{pe}t = 250$ and 750. After that, they coalesce again and form two larger islands at $\omega_{pe}t = 1500$. Finally, they merge again and form the large island at $\omega_{pe}t = 2000$. The width of the island is larger than $10L_{\rm comp}$.

The several coalescences of magnetic islands during the nonlinear stage of the anisotropic tearing instability quasi-periodically create high-energy electrons in the current sheet. Figure 8*a* shows the time development of the number of electrons with energy larger than $100\epsilon_{\rm th}$ at every $50(\omega_{pe}t)$. Figure 8*b* shows the energy spectrum of the electrons with a thin curve at $\omega_{pe}t = 0$ and a thick curve at $\omega_{pe}t = 2000$. The kinetic energy is normalized by the initial thermal energy $\epsilon_{\rm th}$. In the beginning of the simulation, the compression of the current sheet and the enhancement of the tearing instability are associated with the increase of the

number of high-energy electrons in the tearing stage seen in Figure 8*a*. During the coalescence stages, the number of high-energy electrons increases quasi-periodically. The increases are clearly associated with the coalescence of the islands, as compared with Figure 7. It is evident that the acceleration of electrons occurs in the current sheet through the coalescence with magnetic reconnection. The high-energy electrons could be produced through magnetic reconnection and the electric field generated by the motion of the islands during the coalescence process. Some electrons are strongly accelerated, as seen in Figure 8*b*. The maximum energy at $\omega_{pe}t = 2000$ reaches $200\epsilon_{\rm th}$.

The distance traveled by the accelerated electrons can be roughly estimated in a simple way. We assume that one of the energetic electrons is accelerated to almost light velocity, $c$, within $\omega_{pe}t = 2000$, which is the time for this simulation. In the solar corona, as we know, the electron plasma frequency is of the order of 100 MHz, so the simulation time is about 20 $\mu$s. If an energetic electron is accelerated from zero to the light velocity, the required distance is, at maximum, $L \approx 6 \times 10^3$ m. Within this distance, there would be no collisions with protons in the solar corona. The acceleration site of some solar flares may be larger than the spatial scale that we calculate above. Therefore, we expect that the mechanism may accelerate some energetic electrons in solar flares.

## 4. DISCUSSION AND SUMMARY

In this paper, we found one of onset mechanisms of magnetic reconnection in the compressing current sheet. The compression by the plasma inflow induces the temperature anisotropy $T_\perp/T_\parallel \approx 2.1$ through the compression of the magnetic field in the current sheet. During the thinning, magnetosonic shocks are generated and propagate toward outer region. The shocks accelerate some ions in front of them through the surfatron acceleration mechanism. The temperature anisotropy in the current sheet drives the tearing instability, which creates magnetic islands with short wavelengths, $kL_{\rm comp} \geq 1$. The islands vigorously grow in the current sheet through successive coalescence. The process converts the magnetic field energy into particle kinetic energy, and as a result, those electrons that are in the current sheet are well accelerated. Increases of the number of electrons with energy larger than $100\epsilon_{\rm th}$ appear quasi-periodically through the several coalescences of the magnetic islands. At the final stage, all magnetic islands merge into a large one, whose width is larger than $10L_{\rm comp}$.

These results could follow the bursty reconnection model through the secondary tearing instability. As the region where the current sheet is thinning is created through the tearing instability, the magnetic islands are strongly generated at the secondary tearing instability by the enhanced temperature anisotropy in the compressed current sheet. The generated magnetic islands successively coalesce. Through the process, as seen in Figure 8*a*, high-energy electrons are quasi-periodically produced, whose energy is larger than 100 keV if the thermal energy is about 1 keV before a flare. The results from the simulation could be the signature of bursty emissions from solar flares.

During the thinning of the current sheet, the magnetosonic waves are generated and propagate as a shock with the Mach number $M_{\rm A} \approx 1.5$. Some ions are accelerated by surfing the magnetosonic shocks moving to outside of the current sheet. This implies that the acceleration site for the energetic ions is different from that for the accelerated electrons during the flare event. This result may follow the observational result by Hurford et al. (2003). The energetic ions in the region, which is different from the acceleration site for the electrons, are obtained from the previous simulation by Saito & Sakai (2004). The ions are accelerated by the magnetosonic waves generated by the coalescence of two magnetic loops. Both results may imply that energetic ions accelerated during the solar flare event need waves propagating toward the outside of the electron acceleration site, as one of the ion acceleration mechanisms for solar flares. It could be important to study not only the acceleration mechanism directly related to the magnetic reconnection, but also the wave-generation mechanism from the reconnection site. In this simulation, we use the artificial mass ratio $m_i/m_e = 64$. If we assume that the magnetosonic waves are generated in this model with the parameter $m_i/m_e = 1836$, the maximum energy obtained from equation (1) reaches $9.1 \times 10^3\epsilon_{\rm th}$. If we take the thermal energy before a flare to be 1 keV, the accelerated ions have the kinetic energy 9 MeV, which may contribute to the line $\gamma$-ray emission in a solar flare.

As we take account of the third direction parallel to the electric current, the LHDI would be one of the important phenomena for the heating of electrons perpendicular to the magnetic field. We expect that in the three-dimensional system the electrons could be heated preferentially perpendicular to the magnetic field by both LHDI and the compressing effect. Both effects that induce the anisotropic heating would be important in triggering the large-scale magnetic reconnection through the anisotropic tearing instability.

In this study, the heating process during the compression of the current sheet is dealt with as the simple theory of adiabatic heating for electrons. However, to study more detailed processes, we have to consider in future plans the motion of electrons in the regions where there are strong magnetic field gradients (Whipple et al. 1986). We emphasize that we have to consider not only the instabilities in the stable current sheet but also the formation stage of the unstable current sheet for an onset of magnetic reconnection and particle acceleration.

The spatial scale of the acceleration site in this simulation is much smaller than the scale for solar flares. It is impossible to do the simulation with same spatial scale as solar flares, because of a lack of computational power. Further, the mass ratio of ions and electrons should be larger in order to understand realistic phenomena. So, we need to do the simulation with more realistic parameters in future. However, perpendicular heating and the anisotropic tearing instability in the current sheet in collisionless plasma could occur with realistic parameters for the solar corona, so these results may be one of the keys to understanding the acceleration mechanism in solar flares.

We thank the anonymous referee for useful comments. One of authors (S. Saito) was supported by a research fellowship of the Japan Society for the Promotion of Science (JSPS) for young scientists, as a JSPS Research Fellow.

## REFERENCES

Ambrosiano, J., Lee, L. C., & Fu, Z. F. 1986, J. Geophys. Res., 91, 113
Buneman, O. 1993, in Computer Space Plasma Physics: Simulation Techniques and Software, ed. H. Matsumoto & Y. Omura (Tokyo: Terra Scientific)
Burkhart, G. R., & Chen, J. 1989, Phys. Rev. Lett., 63, 159
Daughton, W., Lapenta, G., & Ricci, P. 2004, Phys. Rev. Lett., 93, 105004
Hewett, D. W., Frances, E. F., & Max, C. E. 1988, Phys. Rev. Lett., 61, 893

Hurford, G. J., Schwartz, R. A. Krucker, S., Lin, R. P., Smith, D. M., & Vilmer, N. 2003, ApJ, 595, L77
Karimabadi, H., Daughton, W., & Quest, K. B. 2004, Geophys. Res. Lett., 31, 1
Ohsawa, Y., & Sakai, J. I. 1987, ApJ, 313, 440
Ricci, P., Brackbill, J. U., Daughton, W., & Lapenta, G. 2004, Phys. Plasmas, 11, 4489
Saito, S., & Sakai, J. I. 2004, Phys. Plasmas, 11, 5547
Whipple, E. C., Northrop, T. G., & Birmingham, T. J. 1986, J. Geophys. Res., 91, 4149